Original Article

The effect of ionizing radiation on robotic trajectory movement and electronic components

Sofía Coloma [a,b], Paul Espinosa Peralta [a], Violeta Redondo [a], Alejandro Moroño [c], Rafael Vila [c], Manuel Ferre [a,*]

[a] Centre for Automation and Robotics (CAR) UPM-CSIC, Universidad Politécnica de Madrid, 28006, Spain
[b] Interdisciplinary Research Centre for Security, Reliability and Trust (SnT) in the University of Luxembourg, 1854, Luxembourg
[c] Centre for Energy, Environmental and Technological Research (CIEMAT), Madrid, 28040, Spain

ABSTRACT

Robotics applications are greatly needed in hazardous locations, e.g., fusion and fission reactors, where robots must perform delicate and complex tasks under ionizing radiation conditions. The drawback is that some robotic parts, such as active electronics, are susceptible to radiation. It can lead to unexpected failures and early termination of the robotic operation. This paper analyses the ionizing radiation effect from 0.09 to 1.5 Gy/s in robotic components (microcontrollers, servo motors and temperature sensors). The first experiment compares the performance of various microcontroller types and their actuators and sensors, where different mitigation strategies are applied, such as using Radiation-Hardened (Rad-Hard) microcontrollers or shielding. The second and third experiments analyze the performance of a 3-Degrees of Freedom (DoF) robotic arm, evaluating its components' responses and trajectory. This study enhances our understanding and expands our knowledge regarding radiation's impact on robotic arms and components, which is useful for defining the best strategies for extending the robots' operational lifespan, especially when performing maintenance or inspection tasks in radiation environments.

1. Introduction

Robots are essential when environmental conditions are hazardous for humans. This scenario typically occurs in radiation facilities, space applications, or contaminated environments [1–3]. However, the environment is also sometimes unsuitable for the robot; difficult conditions can compromise the proper functioning of the robotic systems, affecting its electronics, hardware or communications. In this regard, environments with radiation (e.g., particle accelerators, fusion and fission power plants) are among the most challenging places for robotics. Radiation affects electronic devices, temporarily or permanently altering their normal behaviour as a result of Single Event Effects (SEE) or Cumulative Effects (CE) [4–9].

The success of the robotic operation in a radiation environment is greatly conditioned by the proper analysis, selection and placement of the robot's components [10]. It has been especially evidenced in nuclear plants and particle accelerators, where there is high demand for robots to conduct maintenance and decommissioning operations [11–13]. In

these locations, the trend has traditionally been to relocate or move the vulnerable parts of the robot to a safe zone with appropriate radiation protection. However, this approach is sometimes incompatible with the environment's conditions or the robot's operation.

In consequence, the electronics have been improved to extend their durability in ionizing environments. Proof of this is the so-called Radiation Hardened (Rad-Hard) electronic components, which can withstand higher levels of radiation dose and more significant ratios of accumulated radiation [14]. Nevertheless, the expensive catalogue of Rad-Hard electronics is relatively limited and severely regulated under complex political and commercial treaties [15]. Consequently, there must be a trade-off when choosing the type of electronics, such as Rad-Hard vs no Rad-Hard, to apply in robots entering ionizing environments.

This article aims to understand further the effects of ionizing radiation in robotics. It analyses how different electronic components (microcontrollers, servo motors and digital temperature sensors) and 3-Degrees of Freedom (DoF) robotic arm movement are affected over time,

observing their durability and performance. This study also uses different strategies proposed in the literature to study the radiation effects [16,17], such as lead protection and hardening of components. The experimental tests were conducted in a linear particle accelerator at the Centre for Energy, Environmental and Technological Research (CIEMAT, in its Spanish acronym) in Spain.

The structure of the article is as follows. Section 2 explains the related work. Section 3 describes the scenario and experimental setup to test under ionizing radiation. Sections 4, 5 and 6 present three experiments, which are evaluated and analyzed. The work ends with sections 7 and 8, where the discussion, conclusions, and direction of future work are summarized.

2. Related work

2.1. Robot under radiation

Several applications require robots to work under radiation [1,12], such as inspections after nuclear accidents [18], nuclear facility decommissioning [19] or monitoring nuclear facilities [20]. However, only a few articles have studied the effect of radiation on robots. These works have tested individual mobile robot components [19], the radiation tolerance of a commercial robot and its degradation performance [2], and a detection robot [21] or have simulated how radiation affects the robot manipulator performance [22]. We have identified a lack of information on robot performance based on dose rate and type of components used. Therefore, the present research designed low-cost 3-DoF robotic arms to analyze the robot's behaviour depending on the microcontroller, dose rate and irradiation time. Further, we aimed to observe how these elements influence robotic trajectory performance to catalogue the microcontrollers.

2.2. Microcontroller for robotic applications

Microcontroller radiation effects have been extensively reported [5, 6,8,9,23–27]. Various studies have tested different types of microcontrollers under ionizing radiation, where it is possible to observe the variability of duration and degradation in memory, depending on the time and dose rates [24–26]. Additionally, other research has analyzed how Total Ionizing Dose (TID)[1] can vary based on factors such as clock frequency and supply voltage and how this affects the Time Window (TW)[2] of microcontrollers [6]. However, unlike other research, our article compares different types of Commercial Off-The-Shelf (COTS) microcontrollers, some of which have not been previously irradiated in any facility. In addition, we examine the radiation effect on memories and observe the durability and deterioration of the microcontroller when controlling a robotic arm.

2.3. Contributions

This article focuses on better understanding the effect of ionizing radiation on robot components and performance. The main contributions are listed below:

- Testing electronics components (microcontrollers, servo motors, temperature sensors), using mitigation strategies under ionizing radiation (from 0.09 to 1.5 Gy/s) to understand better how they are affected.
- Comparison of the effects and resistance to ionizing radiation depending on the radiation dose and microcontroller type.
- Effect of the evolution of ionizing radiation on robotic arm trajectory.

---

[1] Radiation Absorbed Dose in Grays (Gy).
[2] Period to execute an instruction in a single clock cycle.
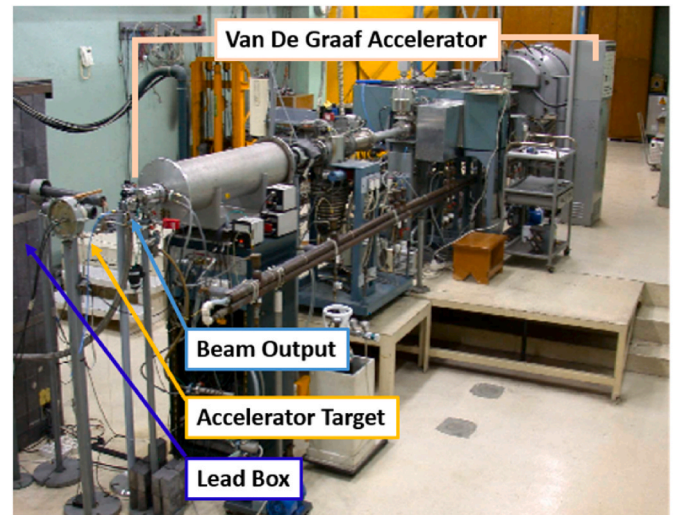
(a)
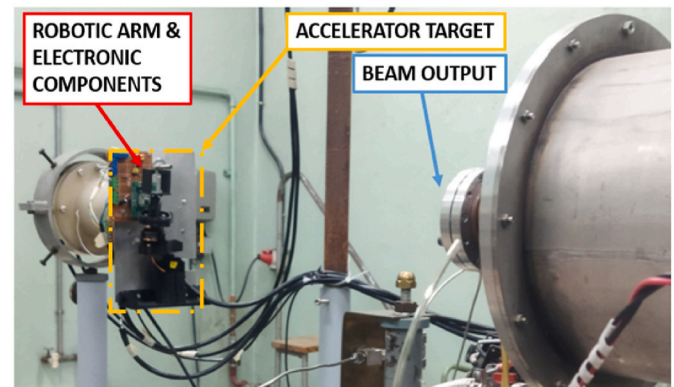
(b)

Fig. 1. (a) General view of the Van de Graaff electron accelerator used for the experiments, (b) Detailed view of the target irradiated during the experiments.

3. Materials and methods

3.1. Testing facility

Mainly, three types of irradiation sources can be used to test the ionizing radiation effects: gamma irradiation facilities, x-ray generators and high-energy electron accelerators. All the tests in this work were carried out using the Van de Graaff electron accelerator at CIEMAT with currents up to 150 μA and energies up to 2 MeV. Further details about the electron irradiation facility can be found at [28]. Samples directly irradiated with electrons were located at the accelerator target location to achieve homogeneous radiation and receive the direct impact of the ionizing electron beam. The electronic components were situated over a 127×200 mm aluminium sheet, which is as close as possible to the emission point of the Gaussian distribution of electrons. Fig. 1 shows a general and detailed view of the facility used during the experiments.

3.2. Testing setup

Communications between the control room and the accelerator target were implemented via a master-slave network over an RS-485 serial line at a 19,200 baud rate. The master controller was a microcontroller located in the control room outside the radiation area, and the microcontrollers in the radiation area behaved as the slaves of the communication line. Fig. 2 shows the communication architecture implemented for the experiments. The master sends movement
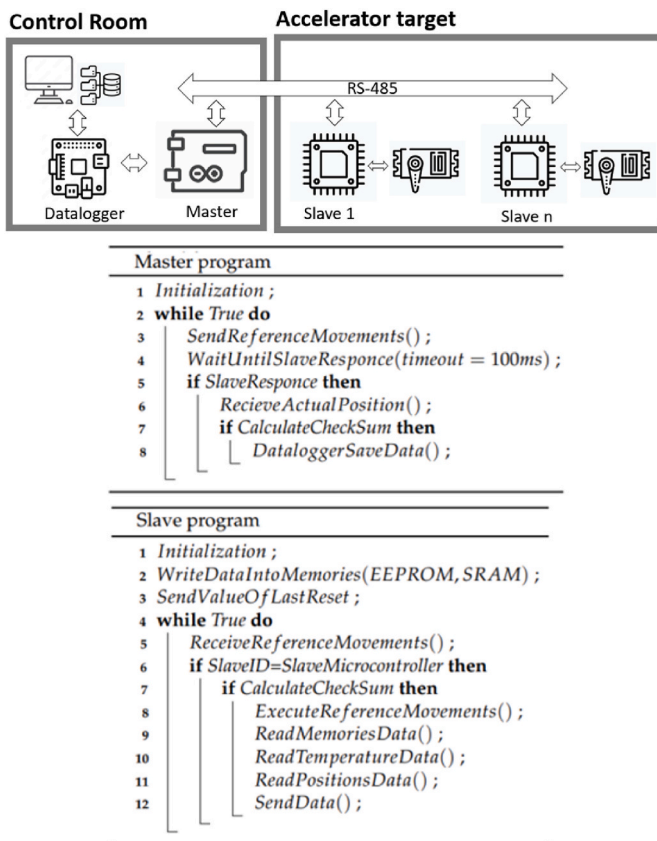
Fig. 2. Communication architecture used for the experiments. A microcontroller acts as a communications master and transmits the information to a data logger managed by a micro-PC. The irradiated microcontrollers in the accelerator room act as slaves to the communication architecture.

commands to the slave and receives information related to the robot's actual position and status of the irradiated microcontrollers. The information received is transferred to a data logger to be saved and subsequently analyzed.

The master sends the robot movement commands to the slaves with the desired final position of the robot. These command movements are processed by the slaves to generate a Pulse Width Modulation (PWM) for the servo motors, which causes the corresponding robot joint displacement. The difference between the desired robot position and the robot's actual position is used to study the radiation effect in the slave microcontrollers. The robot's actual position is obtained from the robot joint potentiometers, and the microcontroller temperature is acquired from digital temperature sensors using the Analog Digital Converter (ADC). All this information is sent to the master, which stores it in the data logger and relays it to a micro-PC. This PC displays the information on a Graphical User Interface (GUI) that the operator uses to monitor the experiments.

The master can detect two kinds of system errors: resets from the slave microcontroller and faults in the communication. The microcontroller slaves generate a reset due to different faults, such as a Watchdog Timer (WDT) or power faults. The communication fault between master and slave typically occurs after several resets in the slave microcontroller. The error analysis was complemented with a specific program to detect memory errors in the irradiated Integrated Circuits (ICs), e.g., if a single particle changes a binary digit of the memory, it could result in a SEE[3] [8]. This application is based on an Error Detection and Correction

---

[3] SEE are caused by one single particle that deposits energy in the electronic device, producing soft or hard errors.

(EDAC) program [29,30], which reads and writes the content of EEPROM, SRAM, and FLASH microcontroller memories. The program saves data and searches for changes in memory.

Furthermore, a system was created to reset microcontrollers through hardware or software remotely. It allows the program to be restarted and the SRAM and EEPROM to be reconfigured based on the detected error. The Flash Memory can only be rewritten by loading the program into the microcontroller, which is only possible when accessing the accelerator at the end of the trials.

3.3. Error metric

The Absolute Trajectory Error (ATE) is applicable in algorithms for robot trajectory estimation [31]. It measures the difference between the ground-truth position and the robot's estimated position simultaneously [32,33], as Equation (1) represents. ATE was used to calculate the error path in the experiments presented in this article, where:

- Ti, is the magnitude of the Euclidean distance along the horizontal plane between the estimated and ground-truth poses at frame i.
- n, number of frames.

$$ATE = \sqrt{\frac{1}{n} \sum_{i=1}^{n} Ti^2} \tag{1}$$

In our work, the ATE was calculated for each cycle or lap. Then, the global ATE corresponds to the mean square value of all the ATE cycles calculated during the experiment.

3.4. Experiments conducted

Three experiments were carried out to analyze and understand the effects of ionizing radiation on passive (microcontrollers with RISC architecture [34], digital temperature sensors) and active (servo motors) robotic components.

- Experiment #1 Analysis of two microcontrollers, servo motors and temperature sensors with mitigation strategies under ionizing radiation.
- Experiment #2 Analysis of robot trajectory under low radiation dose using a non-Rad-Hard microcontroller (ATmega64M1).
- Experiment #3 Comparison of robot trajectory with microcontrollers non-Rad-Hard (ATmega64M1) and Rad-hard (ATmegaS64M1) under radiation.

In Experiment #1, two strategies for radiation mitigation are evaluated: using a radiation-resistant microcontroller and lead shielding. Two Arduino Uno (one shielded and the other unshielded) were selected for their affordability, ubiquity and market availability. In addition, a custom Printed Circuit Board (PCB) with the ATmegaS64M1, a commercially accessible Rad-Hard microcontroller, was also used as a benchmark for radiation resistance with a TID up to 30 Krad. Small COTS servo motors and the LM35 temperature sensor were chosen due to space constraints and their cost-effectiveness and accuracy.

In Experiments #2 and #3, we examined the effect of microcontroller type and radiation dose on the trajectory of the robotic arm. We opted for the ATmega64M1 due to its similarity to the ATmegaS64M1 and its cost, and both microcontrollers come in a Thin Quad Flat Pack (TQFP), which was particularly suitable due to their compact footprint and low profile. The 3-DoF robotic arms were custom designed to fit the accelerator target dimensions, with different joint positions for servo motor orientation. Regarding the radiation aspect, doses were selected based on the availability and capabilities of the accelerator facility.
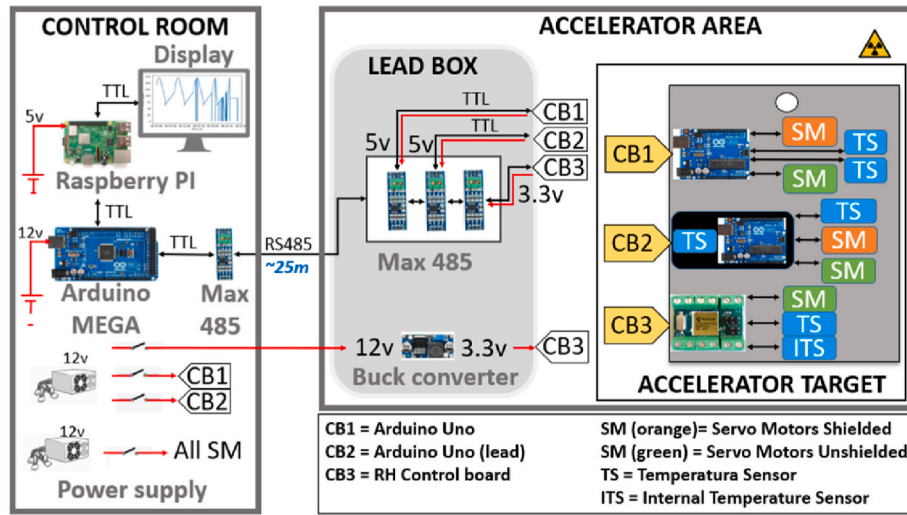
Fig. 3. Experiment #1 setup. The main components in the irradiated area are: ATmega328P without protection (CB1), ATmega328P protected from radiation (CB2) and ATmegaS64M1 (CB3). These microcontrollers control several servo motors and temperature sensors, represented as SM and TS in this figure.
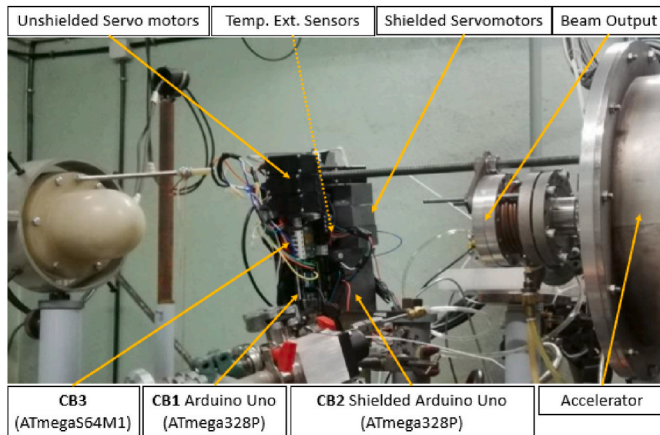

Fig. 4. Accelerator target with irradiated components in experiment #1.

4. Experiment #1: analysis of microcontrollers under ionizing radiation

4.1. Setup

Experiment #1 analyses the behaviour of the microcontrollers (non-Rad-Hard ATmega328P and Rad-Hard ATmegaS64M1) when generating PWM signals for servo motors (Parallax Standard Servo 900–00005) and the environmental temperature provided by two temperature sensors: an external digital temperature sensor LM35 (TO-92 package) and an embedded temperature sensor in the ATmegaS64M1 microcontroller. Fig. 3 shows a diagram of the main components of this experiment, which are as follows:

- Control room with the master microprocessor and micro-PC for saving data and the operator interface.
- Accelerator area with three microcontrollers under different conditions:
  - CB1: ATmega328P (on an Arduino Uno) with a 16 MHz main clock frequency, a 5 V Direct Current (VDC) main power supply, a 5 VDC ADC reference voltage at 125 kHz, and a PWM period of 50 Hz at a 120 KHz clock. It was directly exposed to radiation without any shielding. This microcontroller controls two servo motors (one
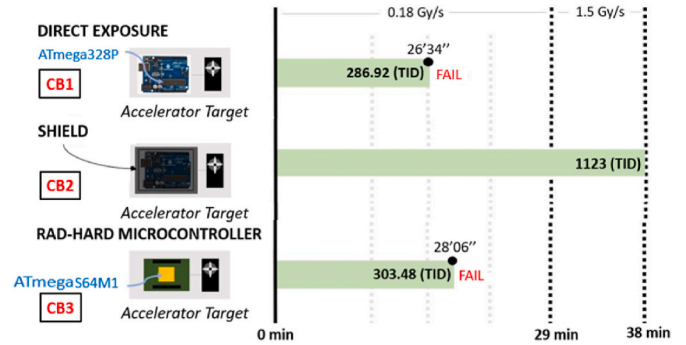
unshielded and the other with 2 mm thick lead shielding). It was also connected to two unshielded external temperature sensors.
  - CB2: ATmega328P (on an Arduino Uno) with the same configuration as CB1 but with 2 mm thick lead shielding. This microcontroller generates PWM signals for two servo motors (one unshielded and the other with 2 mm thick lead shielding). It is also connected to two external temperature sensors (one unshielded and the other with 2 mm thick lead shielding).
  - CB3: ATmegaS64M1 configured with 8 MHz main clock frequency, 3.3 VDC main power supply, 2.56 VDC ADC reference voltage at 125 kHz, and a PWM period of 50 Hz at 120 KHz clock. It is a Rad-Hard microcontroller in a PCB, connected to an unshielded servo motor and two unshielded temperature sensors (integrated and external).

Fig. 5. Microcontrollers used in experiment #1, ATmega328P (Arduino Uno) and ATmegaS64M1 (Rad-Hard).

Table 1
Experiment #1. Dose, TID, ATE error, and time that microcontrollers work. CB1 (ATmega328P without protection), CB2 (ATmega328 P Pb protection), CB3 (ATmegaS64M1 Rad-Hard).

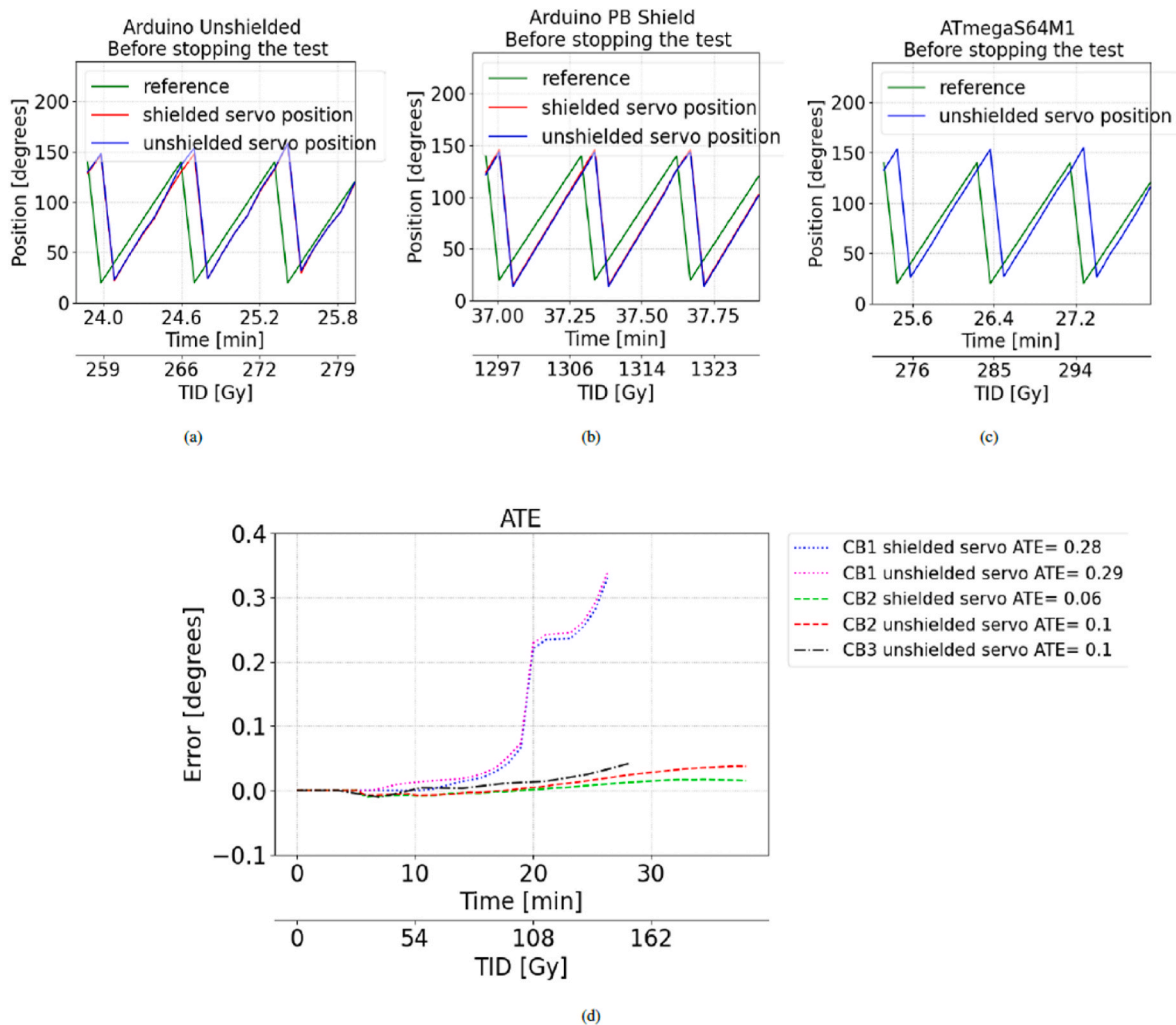| Control Board	Dose [Gy/s]	TID [Grays]	Time [min/sec]	Joints ATE [degrees]	
				Shielded	Unshielded
CB1	0.18	286.92	26′34″	0.28	0.29
CB2	0.18->1.5	1123	>38′	0.06	0.1
CB3	0.18	303.48	28′06″	–	0.1

Fig. 6. Experiment #1. Servo motor position response until the microcontrollers or accelerator stop working in different microcontrollers.
(a) CB1: a dose of 0.18 Gy/s for 26.34 min and TID of 286.92 Gy, **(b)** CB2: a dose of 0.18 Gy/s for 29 min and a dose of 1.5 Gy/s for 9 min and TID of 1123 Gy, **(c)** CB3: a dose of 0.18 Gy/s for 28.06 min and a TID of 303.48 Gy, **(d)** Error positions in ATE metric during the tests. (CB1) ATE is similar in shielded and unshielded servo motors, although ATE should be lower in the shielded servo motor. The error source is due to the microcontroller functionality. (CB2) ATE error shows that the unshielded servo motor differs slightly from the shielded one. It can be observed from minute 20 with 216 Gy of accumulated radiation. In this case, the radiation affectation produces the ATE on servo motors. (CB3) ATE shows a slight increase. The ATE value 0.1 can be compared to that obtained by the unshielded CB2 servo motor.

The experimental setup includes additional components for the power supply devices and signals conversion. Fig. 4 shows a photo of the microcontrollers used in the irradiated area.

4.2. Results

A radiation flow of 0.18 Gy/s was absorbed for 29 min, which was increased to 1.5 Gy/s until minute 38, when we stopped the accelerator. The results are shown in Fig. 5 and Table 1. The CB1 microcontroller (ATmega328P without protection) stopped working due to a severe error after 26 min and 34 s, which corresponds to 286.92 Gy TID. The CB2 microcontroller (ATmega328P with Pb radiation protection) performed correctly over the 38 min of the experiment. It withstood more than 1000 Gy of cumulative radiation, partially retained by the Pb shielding. The CB3 with a Rad-Hard microcontroller (AtmegaS64M1) continued working for 28 min and 6 s, representing 303.48 Gy TID. It stopped working after constant reset signals appeared. The operator attempted to correct the malfunctioning of CB1 and CB3 through software and hardware resets, but restoring a proper microcontroller operation was impossible. In addition, the three microcontroller memories (SRAM, EEPROM and FLASH) were analyzed, although no changes

were detected for this experiment and conditions.

The evolution and response of the shielded and unshielded servo motors were also evaluated. Fig. 6 shows the evolution of the position of the servo motors of the slave microcontrollers when starting the radiation and before stopping the test. Fig. 6a corresponds to CB1 Arduino Uno without protection. It shows somewhat distorted positions on both servo motors before stopping the test due to a microcontroller failure. Fig. 6b corresponds to CB2 Arduino Uno with Pb protection.

The error position observed between the two servo motors is attributed to the influence of the radiation effect. Instead, Fig. 6c, corresponding to CB3 Rad-Hard ATmegaS64M1, shows a minimal distortion in the position values compared to CB1. Although the microcontroller presents unknown reset faults, it can be observed that the degradation produced by the dose received has less impact on the program's operation, and minimal changes exist in the trajectory.

Regarding the temperature sensor response, an increase in temperature values was observed during the experiments. The results for the CB1 temperature sensors are shown in Fig. 7 (blue and magenta lines). The temperature values evolved similarly in both sensors, with a noticeable increase 13 min before the microcontroller failed. This effect is evidence of the electronic degradation of the temperature sensor and
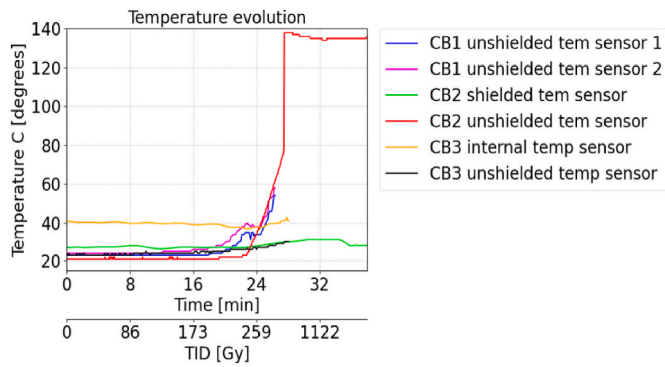
Fig. 7. Experiment #1 Temperature evolution. **(CB1)** Arduino Uno without protection. Dose of 0.18 [Gy/s] for 26 min and 34 s (TID of 286.92 [Gy]). Two unshielded temperature sensors are affected in the same magnitude by the radiation from minute 13. **(CB2)** Arduino Uno with Pb protection. Dose of 0.18 [Gy/s] for 29 min and 1.5 [Gy/s] for 9 min (TID of 1123 [Gy]). Excessive radiation produces a saturation value in the unshielded sensor (red), while the shielded sensor (green) is unaffected. **(CB3)** ATmegaS64M1 Rad-Hard. Dose of 0.18 [Gy/s] for 28 min and 6 s (TID of 303.48 [Gy]). The external temperature sensor changed the value from minute 18, but the magnitude of the change was lower than that for the sensor in CB1. The internal temperature sensor began to change from minute 22, having less significant changes than in the CB1 experiment.

could be used to generate alarms before the communication failure of this component. However, we observed that the temperature values remained stable when the accelerator was stopped and increased again when the irradiation was restored.

The CB2 microcontroller registered higher temperature values with the sensor outside the shield (see Fig. 7; green and red lines). It significantly increased after raising the radiation to 1.5 Gy/s. The values were saturated, corresponding almost to the maximum temperature value of the sensor. Degradation of the internal sensor structure causes the output of the sensor's digital-analogue DAC circuit to be at its highest available voltage. Thus, the control register is always high, and the sensor is permanently damaged. In contrast, the temperature sensor with a Pb shield showed no significant changes from its initial value.

Fig. 7 (black line) shows external sensor temperature values related to CB3. The temperature register is lower than CB1 at the same accumulated radiation dose. For example, the CB3 temperature sensor reached 25 °C after 25 min of irradiation, and the CB1 temperature sensor 42 °C. However, the microcontroller's internal temperature (orange line) sensor shows no substantial changes. As a result, the Rad-Hard microcontroller reduces the accumulative errors when digital

temperature sensors are read.

5. Experiment #2: analysis of robot trajectory ionizing under radiation

5.1. Setup

Experiment #2 analyzes robotic performance using a non-Rad-Hard microcontroller under radiation. It was used with a 3-DoF robot (position micro servo SG90 without radiation protection), controlled with PWM generated by the ATmega64M1 microcontroller (8 MHz main clock frequency, 3.3 VDC main power supply, 2.56 VDC ADC reference voltage at 125 kHz, and a PWM period of 50 Hz at 120 KHz clock). ATmega64M1 also includes an embedded temperature sensor. Figs. 8 and 9 show the main components of this experiment, which are as follows:

- Control room with the master microprocessor and micro-PC for saving data and the operator interface.
- Accelerator area with a 3-DoF robotic arm with a non-Rad-Hard microcontroller.

5.2. Results

For this second experiment, a radiation flow of 0.09 Gy/s was generated for 52 min. Less radiation dose was selected to observe its impact on the elements and the robotic functionality. The non-Rad-Hard ATmega64M1 microcontroller reached 282.15 Gy TID; the results are
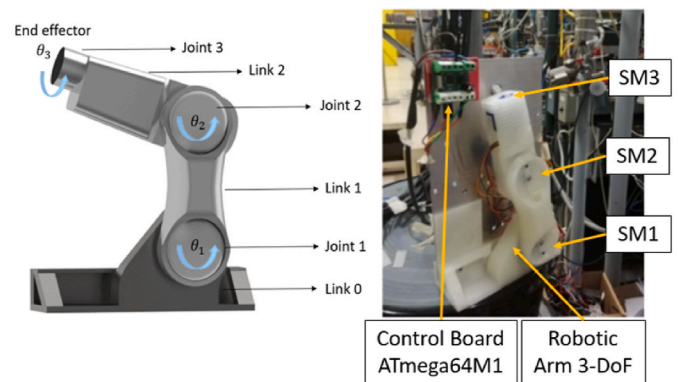

Fig. 9. 3-DoF robotic arm from Experiment #2. Left-hand image: kinematic configuration of the robot. Right-hand image: setup used during the radiation.
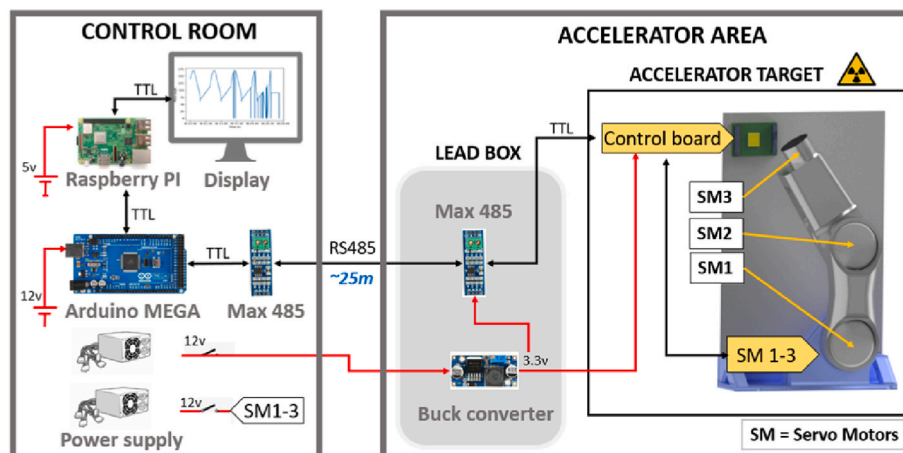

Fig. 8. Experiment #2 setup. Control room with the same structure as in Experiment #1 and a 3-DoF robotic arm with rotational joints in the accelerator area.

Table 2
Results of Experiment #2, representing the radiation dose on the microcontroller, TID, ATE and work time.

Control Board	Dose [Gy/s]	TID [Grays]	Time [min/sec]	Joints ATE [degrees]		
				J1	J2	J3
ATmega64M1	0.09	282.15	52′15″	0.09	0.12	0.8

shown in Table 2.

The microcontroller produced a constant reset signal seconds before failure, stopping the correct functioning of the robot system. The microcontroller current rose from 5.20 mA to 8.49 mA, suggesting a possible impedance reduction or leakage, which might have caused voltage problems. The microcontroller memories (SRAM, EEPROM, and FLASH) were also checked, but no changes in data were observed.

The servo motor response of each robotic joint was analyzed for this experiment. For this purpose, the microcontroller of the robotic arm was programmed to generate a repetitive trajectory. It enabled us to compare the deviation (i.e., error) from the ideal trajectory over time. Fig. 10 shows the position values at the end of the test and the ATE metric across the experiment.

The results show a clear difference in position between Joints 1, 2,

and 3. Specifically, Joint 3 (Fig. 10c) exhibits notable position changes. It occurred as a result of the radiation beam's impact on the electronics of the servo motor at Joint 3, which is positioned perpendicularly compared to other servo motors, as shown in Fig. 9. Its electronics were more susceptible to radiation exposure due to the servo motor components configuration. Nonetheless, the three joints present variation in ATE across the experiment, with Joints 1 and 2 increasing slightly, as shown in Fig. 10 represents.

The servo motor in Joint 3 has apparent electronic damage. It might have been accentuated by the deterioration of the microcontroller and the accumulated radiation dose, which may have affected the other servos. Furthermore, this robotic arm was configured to follow a predefined reference trajectory, with the servo motors moving accordingly during the experiment. This robot trajectory was obtained by applying the forward kinematics [35] without considering Joint 3.

The outcomes of this analysis are shown in Fig. 11. The first position errors were detected after 30–35 min of irradiation, corresponding to a cumulative radiation dose of 162–189 Gy. This position error increases and is notable after 40 min of radiation, although communications continue for 12 min more, i.e. until it reaches 52 min of irradiation. The program was executed correctly, given that the robot repeated the movement cycle continuously. However, we observed that the data handled by the microcontroller was altered since position errors were
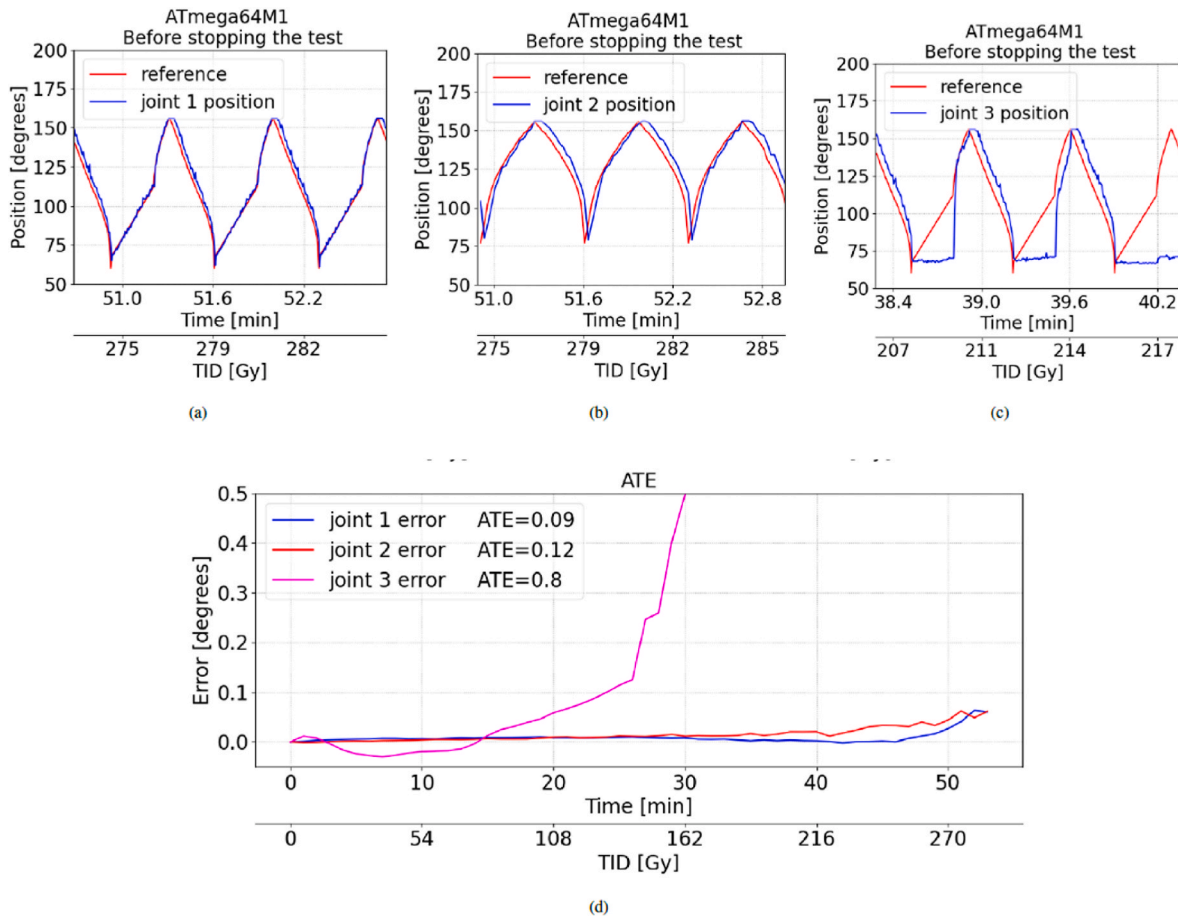

(a) (b) (c)

(d)

Fig. 10. Experiment #2. Servo motors position response with ATmega64M1 microcontroller with a dose of 0.09 Gy/s for 52.15 min and TID of 282.15 Gy. (a, b, c) positions until the microcontrollers or the accelerator stop working. (d) Error positions in ATE metric during the tests.
(a) Joint 1 with a slight lag and undulations of the position. **(b)** Joint 2 with a reference value displacement and small waves. **(c)** Joint 3 with trajectory position errors before the other joints. **d)** Joint 1: ATE representation does not show significant differences between minutes 0 and 42 (226.8 Gy of cumulative radiation dose). Then, we can see how the error increases and the position of the servo motors differ slightly from the reference values. Joint 2: ATE representation shows a little increase in the error until minute 40 (216 Gy of accumulated radiation dose). After that, the error increases faster for 10 min. The middle graph shows a deviation and ripple trajectories from minute 51 (271 Gy of accumulated radiation dose) until the end of the test. Joint 3: ATE has a considerable error increase from minute 25 to 50 (135–270 Gy of accumulated radiation dose). The error becomes more prominent, with a more significant difference between reference and position feedback values.
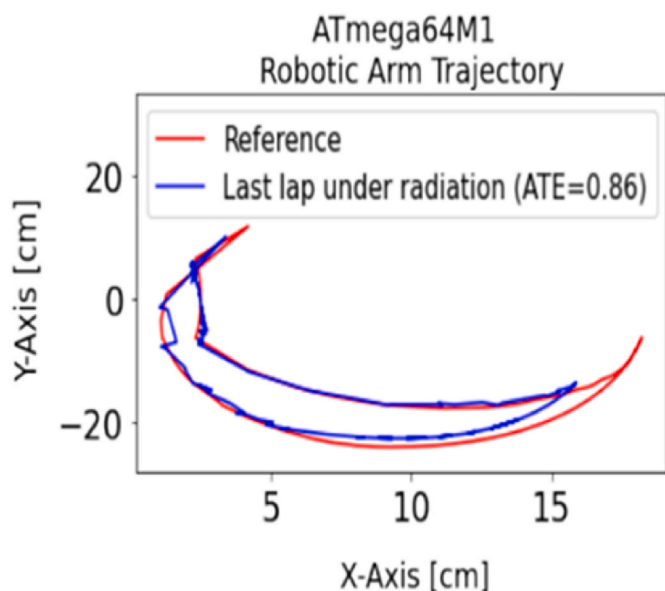
Fig. 11. Experiment #2. Comparison of robot trajectories during the experiment. The red line represents the reference trajectory. The blue line is the trajectory obtained at minute 50 of the experiment, with a cumulative radiation dose of 270 Gy. The ATE was calculated using the position values from the last lap and the reference value.
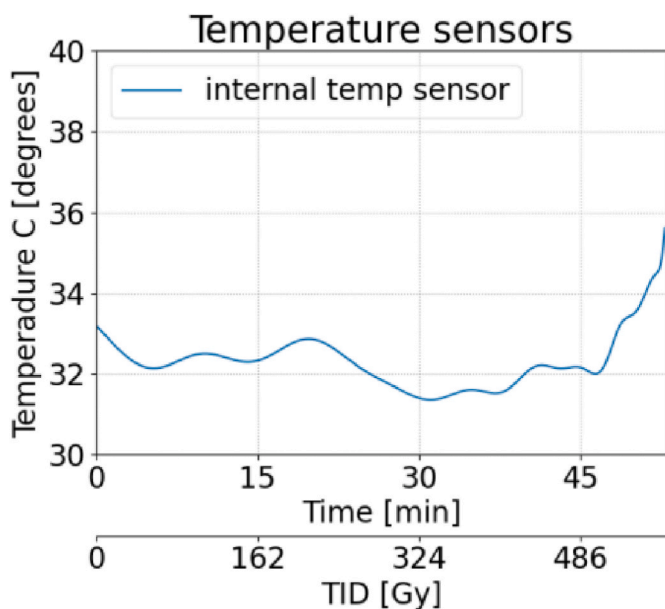

Fig. 12. Experiment #2 ATmega64M1 internal temperature evolution. The temperature value shows no significant changes until minute 45 (234 Gy of accumulated radiation dose). After this time, the value of temperature increases until the microcontroller fails.

detected incrementally. It was noted that the microcontroller started to deteriorate after 30 min of irradiation. This deterioration may have occurred because the processor executes the program's instructions in a larger TM allowed [6], causing data corruption.

The problem with corrupt data is that it provokes a random position error without jumps or abrupt movements. This fact is due to the robot's inertia and the trajectories' continuity. The robot error position is not cumulative and induces a robot trajectory oscillating around the reference trajectory.

The response of the internal temperature sensor of the ATmega64M1

microcontroller was evaluated for this experiment. Fig. 12 shows that the temperature varies, becoming more accentuated from minute 45 (486 Gy of accumulated radiation dose) due to the radiation effect and microcontroller degradation.

6. Experiment #3: comparison of robot trajectory with microcontrollers under ionizing radiation

6.1. Setup

Two different microcontrollers were used for experiment #3: the ATmega64M1 (conventional) and ATmegaS64M1 (Rad-Hard version). Both are set up with an 8 MHz main clock frequency, 3.3 VDC main power supply, 2.56 VDC ADC reference voltage at 125 kHz, and a PWM period of 50 Hz at 120 KHz clock. The communication architecture and setup are similar to those in experiment #2, represented in Fig. 8. However, experiment #3 uses another 3-DoF robotic arm, as shown in Fig. 13. The configuration and servo motors differ. Joints 1 and 2 use position servo motors (Grove Servo 316010005) and Joint 3 velocity servo motors (Hitech HS-55). Additionally, after stopping the test, the memories were downloaded to check possible byte changes.

6.2. Result

Table 3 details the main information related to this experiment #3, where the radiation flow was 0.18 Gy/s. The ATmega64M1 lasted 20 min, reaching 218 Gy TID. While the Rad-Hard version, ATmegaS64M1, extended its operating duration to 28 min and a TID of 311 Gy, until the microcontroller failed. Both microcontrollers execute the same program, which implements a semi-circular trajectory. The position-controlled servos follow a defined path, going from 0 to 90° and back to 0°, increasing and decreasing degree by degree. The velocity-controlled servo is set at 180° per second. Each servo motor's position and velocity values were checked for the joints in this experiment.

Fig. 14a–d show the information extracted from Joint 1, Fig. 14b–e for Joint 2 and Fig. 14c–f for Joint 3. The results reveal an evident distortion compared to the position of the servo motors in the previous experiments (Fig. 10). This means a higher radiation dose produces more corrupted data, and the trajectory oscillates around the ideal trajectory. Additionally, the error of the velocity response in both microcontrollers is higher after radiation exposure, given that the movement of Joint 3 was closer to the radiation beam.

The robotic arm trajectory was also evaluated, as the trajectory evolution (before and under radiation) was saved. The position of the robot's end effector was calculated by direct kinematics [35]. Fig. 15 shows the trajectories with these microcontrollers, where we obtained results consistent with previous experiments. In particular, Fig. 16 shows the evolution of the robot trajectory error, ATE, during the experiments. As we can see, both microcontrollers present improper functionality: ATmega64M1 (non-Rad-Hard) after 20 min of radiation and ATmegaS64M1 (Rad-Hard) after 28 min of radiation. Moreover, the robot position error increases some minutes before: at minute 7 (67.2 Gy of accumulated radiation dose) for the ATmega64M1 and minute 20 (192 Gy of accumulated radiation dose) for the ATmegaS64M1.

Unlike the other experiments, changes in data memory were detected by reading all available memories. ATmega64M1 presented 11,160 corrupted bytes in FLASH memory at minute 28 (217.7 Gy of accumulated radiation dose), while corrupted memory data in ATmegaS64M1 (Rad-Hard) were not detected.

The outcomes for the internal temperature sensor response of the microcontrollers are shown in Fig. 17. ATmega64M1 temperature sensor (red line) presents a temperature increase from minute 6 (57.6 Gy of accumulated radiation dose). However, it becomes more critical from minute 19 (182.4 Gy of accumulated radiation dose), where the value increases significantly after the test was stopped for a few minutes due to a microcontroller malfunction.
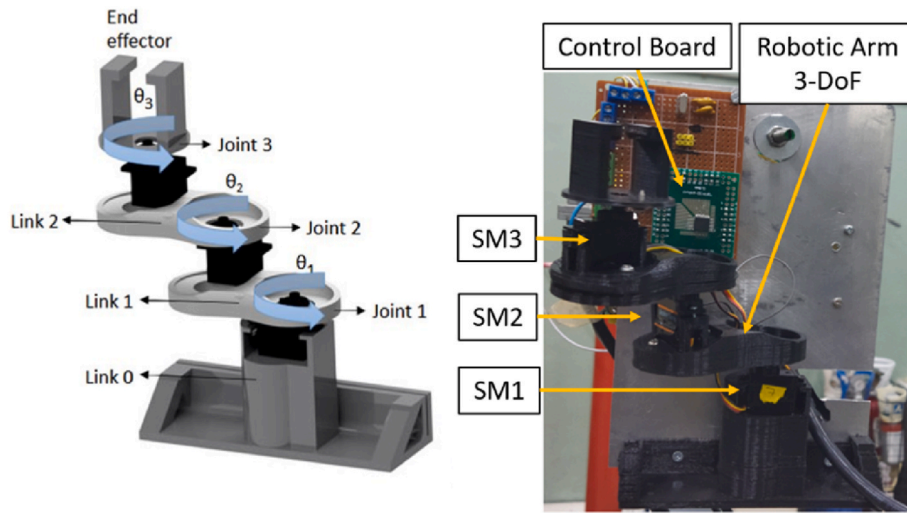
Fig. 13. Setup for experiment #3. Left-hand image: 3-DoF robot configuration. Right-hand image: robotic arm and its components in the accelerator target.

Table 3
Results of Experiment #3, representing the radiation dose on the microcontroller, TID, ATE and work time.

Control Board	Dose [Gy/s]	TID [Grays]	Time [min/sec]	Joints ATE [degrees]		
				J1	J2	J3
ATmega64M1	0.18	218.88	20′16″	0.54	0.66	1.21
ATmegaS64M1 (Rad-Hard)	0.18	311.22	28′49″	0.15	0.30	0.46

Joints 1 position response. The trajectory of ATmega64M1 begins to present ripples from minute 8 (76.8 Gy of accumulated radiation dose). In comparison, the ATmega64M1 (Rad-Hard) presents smaller ripples and peaks from minute 21 (201.6 Gy of accumulated radiation dose). ATE representation shows that ATmega64M1 (ATE = 0.54) has a more significant error value than ATmegaS64M1 (ATE = 0.15).

Joints 2 position response. The behaviour of the trajectory is similar to Joint 1. However, the ATE value is higher because Joint 2 is close to the radiation beam, and the servo motor absorbs more radiation. The trajectory of ATmega64M1 begins to present ripples from minute 5 (54 Gy of accumulated radiation dose), while the ATmega64M1 (Rad-Hard) presents smaller ripples and peaks from minute 21 (201.6 Gy of accumulated radiation dose). The ATE representation shows that ATmega64M1 (ATE = 0.66) has a higher error value than ATmegaS64M1 (ATE = 0.3).

Joints 3 velocity response. The ATE value is higher than for Joints 1 and 2 because Joint 3 is closer to the radiation beam. The trajectory of ATmega64M1 begins to present a different velocity value from minute 7 (67.2 Gy of accumulated radiation dose). Instead, the ATmega64M1 (Rad-Hard) differs significantly from minute 20 (192 Gy of accumulated radiation dose). The right-hand graph (ATE representation) shows that ATmega64M1 (ATE = 1.21) has a higher error value than ATmegaS64M1 (ATE = 0.46).

For ATmegaS64M1, the results are different (blue line). The sensor presents a temperature rise from minute 11 (105.6 Gy of accumulated radiation dose). Although, it is more noticeable at minute 25, before the end of the test. The results evidence that as the temperature of the Rad-Hard microcontroller rises, the structure begins to be damaged, and it is more stable than de non-Rad-Hard version.

7. Discussion

In this section, the following points describe the general findings and observations obtained from the tests. In addition, Table 4 summarises the experiment's findings and how ionizing radiation affected the electronic components.

● **Microcontrollers:** using a Rad-Hard microcontroller (ATmegaS64M1) proved effective in withstanding higher levels of ionizing radiation (up 311.2 Gy of TID) and maintaining functionality longer, i.e. between 8% and 35% more concerning the other tested microcontrollers (ATmega328P with 286.92 Gy and ATmega64M1 with 218.88 Gy). However, the lead shielding protected the microcontroller significantly, preventing failure and keeping the operation under radiation exposure. Furthermore, the test revealed that radiation levels are critical in determining their lifespan.

● **Servo motors:** experienced position deviations and errors in response to radiation exposure. They provided less positioned error when the microcontroller was shielded, effectively mitigating radiation effects and maintaining proper functionality. The location of servo motors on the accelerator target has a notable influence, as the radiation beam affects the electronics differently based on their positioning. In addition, the impact of radiation on the servo motor position varied depending on the microcontroller type. In this case, servo motors controlled by Rad-Hard microcontrollers demonstrated better performance and less degradation.

● **Temperature sensors:** exhibited increased temperature values during irradiation, indicating electronic degradation. Instead, the error remained with the same value when the accelerator was stopped. The error sensor temperature increased with radiation exposure and increasing dose, with potential implications for reliability and long-term performance. In some cases, the unshielded ATmega328P microcontroller showed high-temperature errors. The embedded temperature sensors in the microcontroller showed less error than the external sensor.

● **Robotic arm trajectory**: has shown better performance with Rad-Hard AtmegaS64M1. At a 0.18 Gy/s dose rate, it showed greater trajectory stability during the first ~19 min (200–220 Gy), surpassing the non-Rad-Hard version, which remained stable for only ~7 min (70–80 Gy). The Rad-Hard also minimized ATE, where Joint 1 experienced 0.15° ATE, Joint 2 experienced 0.3° (causing a trajectory change of 0.9 cm) and Joint 3 deviated 12°/s. Instead, the non-Rad-Hard presented in the robot trajectory an ATE of 0.54° in Joint 1, 0.66° in Joint 2 (causing a displacement of 2.0 cm) and a deviation
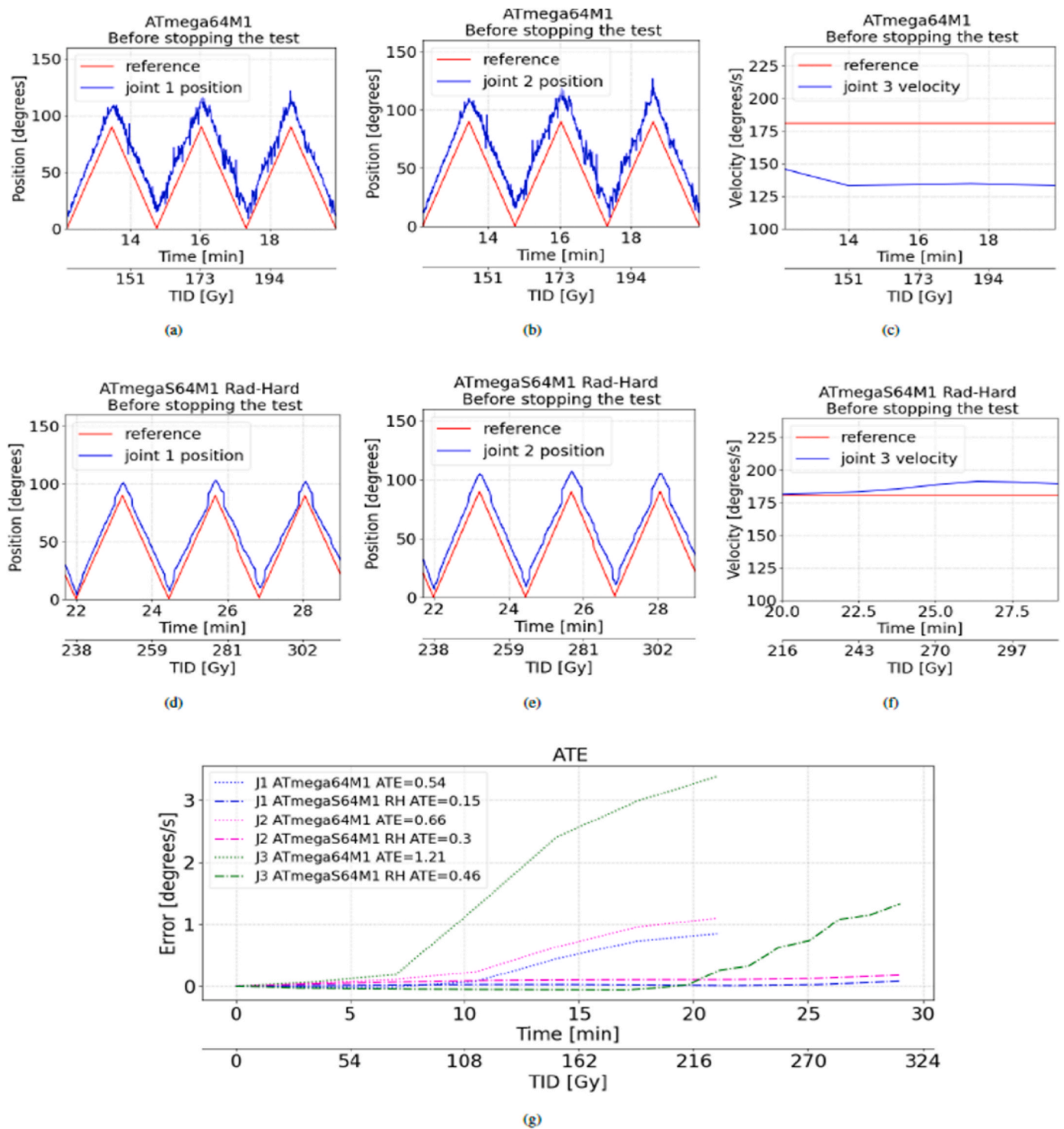
Fig. 14. Experiment #3 Evolution of ATmega64M1 (a,b,c) and ATmegaS64M1 (d,e,f) servo motors. (g) ATE response to each joint.
(a) Joint 1: a dose of 0.18 Gy/s for 20.16 min and TID of 218.88 Gy. (b) Joint 2: a dose of 0.18 Gy/s for 20.16 min and TID of 218.88 Gy. (c) Joint 3: a dose of 0.18 Gy/s for 20.16 min and TID of 218.88 Gy. (d) Joint 1: a dose of 0.18 Gy/s for 28.49 min and TID of 311.22 Gy. (e) Joint 2: a dose of 0.18 Gy/s for 28.49 min and TID of 311.22 Gy. (f) Joint 3: a dose of 0.18 Gy/s for 28.49 min and TID of 311.22 Gy. (g) ATE representation to both microcontrollers and joints.

of 37°/s at Joint 3. In contrast, at a reduced dose rate of 0.9 Gy/s, the main servo motors for the robot trajectory show an ATE of 0.09° in Joint 1, 0.12° in Joint 2 (causing a shift of less than 0.1 cm in the trajectory) and a deviation greater than 0.8° in the Joint 3. The last one was the most affected because of its position.

● **Mitigation strategies:** Rad-Hard microcontrollers and lead shielding have shown benefits under ionizing radiation, wherein the
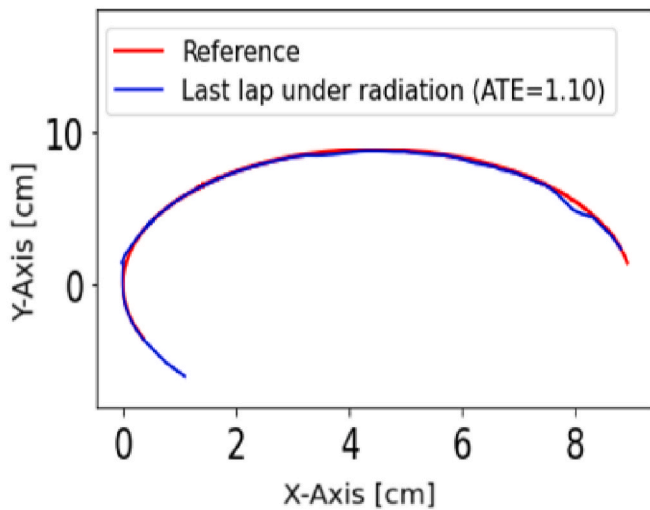
shielding of electronic components has been more effective and economical.

8. Conclusions

This work evaluated the effect of ionizing radiation (0.09–1.5 Gy/s) on different components of robotic systems, including microcontrollers,
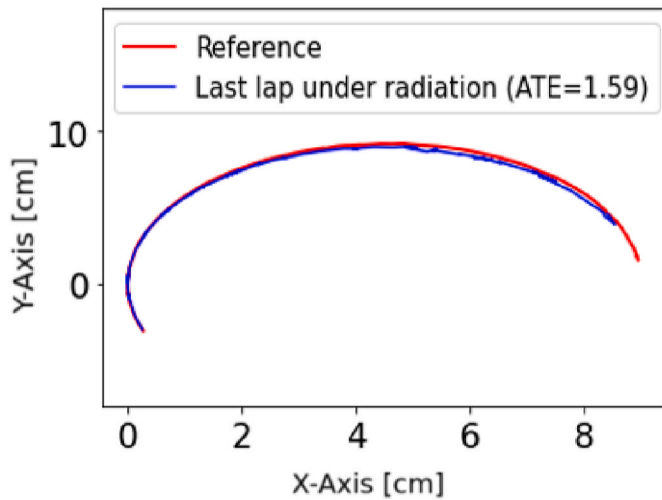
(a)   The trajectory for ATmega64M1.

(b) The trajectory for ATmegaS64M1 Rad-Hard.

Fig. 15. Examples of trajectories executed in experiment #3. For microcontroller ATmega64M1, the radiation absorbed at the beginning of the last lap under radiation was 290Gy, while for the ATmegaS64M1, the dose absorbed was 380Gy. The ATE was calculated using the position values from the last lap and the reference value.

servomotors, and temperature sensors. In addition, the effects of radiation on the trajectory of two 3-DoF robotic arms were analyzed.

The findings have shown that the Rad-Hard microcontroller tolerates more radiation and provides more signal stability to connected sensors or actuators than a conventional one. However, shielding the microcontroller has demonstrated more resistance over time and less impact on the actuators' and sensors' performance. This fact highlights the importance of using techniques to mitigate the radiation effect.

In addition, the research explored the influence of different radiation doses and microcontrollers on robotics performance. The effectiveness of robotic arms' trajectory and performance in harsh environments highly depends on the electronics type, the configuration and the radiation dose. In our tests, the Rad-Hard AtmegaS64M1 microcontroller outperformed the non-Rad-Hard in stability and accuracy under high radiation doses.
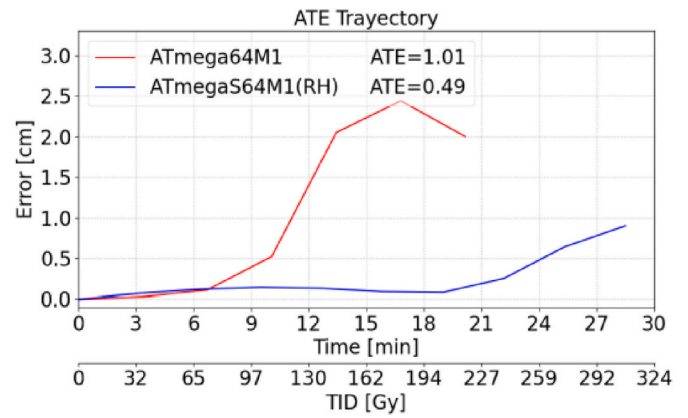

Fig. 16. Evolution of the error in robot trajectories during experiment #3 (0.180 Gy/s). The ATmega64M1 (red line) performs adequately for the first 7 min (75.6 Gy of accumulated radiation dose). The error grows considerably until minute 17 (183.6 Gy of accumulated radiation dose) and then decreases until functionality fails at minute 20 (218.88 Gy of accumulated radiation dose). The decrease in the error is due to the change in the servo motor direction. The ATmegaS64M1 Rad-Hard (blue line) shows proper performance for the first 18 min (182.4 Gy of accumulated radiation dose), and then the error increases until minute 28 when functionality fails.
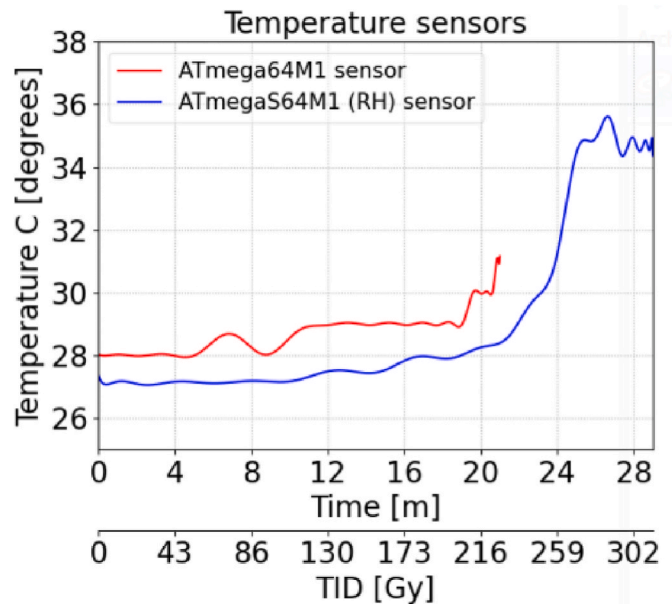

Fig. 17. Experiment #3 ATmega64M1 and ATmegaS64M1 internal temperature evolution. The picture shows the same behaviour as the last tests (increasing its value as more radiation is absorbed). However, the internal sensor of Rad-Hard presents fewer variations until the sensor's internal structure begins to be damaged.

The tested active (servo motors) and passive (temperature sensors) components exhibit degraded responses when the microcontroller suffers internal damage. This phenomenon can serve as an early warning signal, alerting operators to the deteriorating state of the microcontroller or acting automatically to adjust internal configurations, states machines and redundancy microcontrollers.

This study underlines the importance of using mitigation strategies to minimize radiation's effect and thus improve robotic systems' performance and reliability in hostile environments. The results provide valuable information for designing and implementing robotic systems in various applications, ultimately advancing the field of robotics in

Table 4
Summary of the three experiments' results per microcontroller. It presents the time, the dose, the signal reset and the failure reason, the maximum temperature reached, and the ATE (ATE<0.5 = Low, 0.5 < ATE<1.0 = Medium, ATE>1.0 = High) to have a general overview of the results.

Microcontroller	Test	Dose [Gy/s]	TID [Gy]	Time [min/sec]	Fails detected	Servo motor position degradation (Level-ATE)	Robotic Arm trajectory last lap degradation (Level-ATE)	Temperature error init temp-final temp
ATmega328P	#1	0.18	286.92	26′34″	Fatal error UC stop working	Low- 0.29 Low – 0.28 (shielded)	–	Ext. Sen 1: 30 °C Ext. Sen 2: 33 °C
ATmega328P (lead shielded)	#1	From 0.18 up to 1.5	1123	>38′	No fail	Low – 0.1 Low – 0.06 (shielded)	–	Ext. Sen 1: 2 °C (shielded) Ext. Sen 2: 117 °C
ATmegaS64M1	#1	0.18	303.48	28′06″	WDT and unknow reset	Low – 0.1	–	Int. Sen: 2 °C Ext. Sen: 5 °C
	#3	0.18	311.22	20′16″	WDT and unknow reset	Joint 1: Low – 0.15 Joint 2: Low – 0.30 Joint 3: Low – 0.46	Low – 1.10	Int. Sen: 8 °C
ATmega64M1	#2	0.09	282.15	52′15″	WDT and unknow reset	Joint 1: Low – 0.09 Joint 2: Low – 0.12 Joint 3: Medium – 0.8	Medium – 0.86	Int. Sen: 3 °C
	#3	0.18	218.88	20′16″	WDT and unknow reset Corrupted bytes in FLASH memory	Joint 1: Medium – 0.54 Joint 2: Medium – 0.66 Joint 3: High – 1.21	High – 1.59	Int. Sen: 3 °C

environments with ionizing radiation.

8.1. Future work

In future work, the goal is to design robust and low-cost small inspection robots specifically designed to operate in environments with high ionizing radiation due to the need to prevent humans from being exposed to these hazardous areas. Also, create an alarm system using low-cost active components to prevent critical damage in robots. These robots and systems would undergo rigorous testing under high radiation doses to assess their performance and durability.

To achieve this, additional testing involving irradiation of multiple microcontrollers with different power supply values, clock frequencies, and radiation doses is necessary to assess the constraints and their maximum operational lifetime. Further, we pretend to carry out experiments to investigate the effects of ionizing radiation on the performance of PWM signals and ADC readings, as it can interfere with the performance and accuracy of electronic components.

In addition, it is proposed to explore how to adapt and effectively apply the GEMMA guide [36] in environments with high ionizing radiation, which aims to optimize the design of state machines with redundancy in case of microcontroller failure. It will improve performance, reduce critical failures, and maximize the uptime of electronic and robotic systems in radiation environments.

On the other hand, an important area for future lines of research is the integration of Artificial Intelligence (AI), which could detect early failures, optimize performance, adapt to changing conditions and make intelligent decisions to prolong the operational life of the systems, and also prevent abnormal behaviours in robots when operating in critical areas subjected to radiation.

Declaration of competing interest

The authors declare that they have no known competing financial interests or personal relationships that could have appeared to influence the work reported in this paper.

Acknowledgements

References

[1] R. Smith, et al., Robotic development for the nuclear environment: challenges and strategy, Robotics (2020).
[2] K. Zhang, et al., Radiation tolerance testing methodology of robotic manipulator prior to nuclear waste handling, Frontiers in Robotics and AI 7 (2020).
[3] S. Coloma, et al., Enhancing rover teleoperation on the moon with proprioceptive sensors and machine learning techniques, IEEE Rob. Autom. Lett. 7 (2022).
[4] F. Faccio, et al., COTS for the LHC radiation environment: the rules of the game, in: LEB 2000 Conference Krakow, Book of Abstracts, 2000, p. 50.
[5] B. Todd, S. Uznanski, Radiation Risks and Mitigation in Electronic Systems, 2016 arXiv preprint arXiv:1607.01573.
[6] Z. Diggins, et al., Total-ionizing-dose induced timing window violations in CMOS microcontrollers, IEEE Trans. Nucl. Sci. 61 (2014).
[7] F. Faccio, et al., Radiation effects in the electronics for CMS, Tutorial Script, CERN (1999).
[8] E. Petersen, Single Event Effects in Aerospace, John Wiley & Sons, 2011.
[9] S.J. Gaul, et al., Integrated Circuit Design for Radiation Environments, John Wiley & Sons, 2019.
[10] S. Coloma, et al., Remote Handling Maintenance of Beam Dump in IFMIF-DONES, Fusion Engineering and Design, 2021.
[11] M. Di Castro, et al., Cerntauro: A Modular Architecture for Robotic Inspection and Telemanipulation in Harsh and Semi-structured Environments, IEEE Access, 2018.
[12] I. Tsitsimpelis, et al., A review of ground-based robotic systems for the characterization of nuclear environments, Prog. Nucl. Energy 111 (2019).
[13] G. Micciche, et al., The remote handling system of IFMIF-DONES, Fusion Eng. Des. 146 (2019).
[14] J.D. Cressler, et al., Extreme Environment Electronics, CRC Press, 2017.
[15] P.R. Villa, et al., Analysis of single-event upsets in a microsemi ProAsic3E FPGA, in: 2017 18th IEEE Latin American Test Symposium (LATS), IEEE, 2017.
[16] G. Foucard, Handbook of Mitigation Techniques against Radiation Effects for Asics and Fpgas, CERN [online], Jan, 2012.
[17] C. Peng, et al., Radiation-hardened 14T SRAM bitcell with speed and power optimized for space application, IEEE Trans. Very Large Scale Integr. Syst. 27 (2018).
[18] M.S. Muktadir, et al., Development of a radiation detection measuring and monitoring mobile facility with wireless autonomous robots, in: The Proceedings of the International Conference on Nuclear Engineering, ICONE), 2019.
[19] B. Bird, et al., Vega—a small, low cost, ground robot for nuclear decommissioning, J. Field Robot. (2021).
[20] B. Bird, et al., A Robot to Monitor Nuclear Facilities, IEEE Robotics & Automation Magazine, 2019.
[21] F. Chen, et al., The radiation tolerance design and test of a tele-controlled robot, Nucl. Electron. Detect. Technol. 36 (2) (2016).
[22] S. Li, et al., Radiation effect on the performance of robot manipulator, Int. J. Mechatron. Autom. 6 (2017).
[23] C. Sharma, et al., Impact of Gamma Radiation on 8051 Microcontroller Performance, Nuclear Engineering and Technology, 2022.
[24] T. Fried, et al., Radiation testing of low cost, commercial off the shelf microcontroller board, Nucl. Eng. Technol. 53 (2021).
[25] M. Nancekievill, et al., Radiation tolerance of commercial-off-the-shelf components deployed in an underground nuclear decommissioning embedded system, in: 2016 IEEE Radiation Effects Data Workshop (REDW), IEEE, 2016.
[26] J. Navarrete, et al., Irradiation Measurements of the Hitachi H8S/2357, MCU, 2003.

[27] S. Keller, et al., DD1: a QDI, radiation-hard-by-design, near-threshold 18uW/MIPS microcontroller in 40nm bulk CMOS, in: 2015 21st IEEE International Symposium on Asynchronous Circuits and Systems, IEEE, 2015.

[28] CIEMAT electron accelerator [Online]. Available, http://www.fusion.ciemat.es/competitive-access-to-facilities/electron-accelerator/. (Accessed 19 June 2023).

[29] S. Coloma, Methods, Strategies and Application Cases for Robotic Telemanipulation in Hazardous Environments, Ph.D. Thesis, Universidad Politécnica de Madrid, Madrid, Spain, 2020.

[30] F.G. Leite, et al., Ionizing radiation effects on a COTS low-cost RISC microcontroller, in: 2017 18th IEEE Latin American Test Symposium (LATS), IEEE, 2017, pp. 1–4.

[31] P. Espinosa Peralta, et al., Performance analysis of localization algorithms for inspections in 2D and 3D unstructured environments using 3D laser sensors and UAVs, Sensors (2022).

[32] J.O. Sturm, A benchmark for the evaluation of RGB-D SLAM systems, in: 2012 IEEE/RSJ International Conference on Intelligent Robots and Systems, IEEE, 2012.

[33] Rawseeds, Absolute trajectory error, Available: http://www.rawseeds.org/rs/methods/view//9. (Accessed 19 June 2023).

[34] C. Kuhnel, AVR RISC Microcontroller Handbook, Newnes, 1998.

[35] S. Kucuk, Z. Bingul, Robot Kinematics: Forward and Inverse Kinematics, INTECH Open Access Publisher London, UK, 2006.

[36] G. Cloutier, J.-J. Paques, Gemma, the Complementary Tool of the GRAFCET, Programmable Control and Automation Technology Conference and Exhibition, 1988.